Development of a groundwater-drawdown function to estimate spatially varying land subsidence: a case study of the Choshui River basin, Taiwan

Hone Jay Chu[1], Muhammad Zeeshan Ali[1], and Tom Burbey[2]

[1]National Cheng Kung University
[2]Virginia Tech

April 28, 2020

Abstract

Land subsidence caused by groundwater overexploitation is a critical global problem. Spatial distribution of land subsidence is crucial for environmental management and land planning due to the sensitive nature of land-surface gradients. Given the nonlinear relationship of subsidence and long-term drawdown from groundwater exploitation, and the heterogeneity of the aquifer in the Choshui River alluvial fan, a developed spatial regression model can effectively estimate nonlinear and spatially varying subsidence. That is, the root-mean-square-errors (RMSEs) of annual subsidences are less or equal to 0.8 cm. Considering various data inputs in the Choshui River alluvial fan, the spatial regression model offers a robust method for estimating the spatial patterns of subsidence using drawdown as observations. Results show that the largest water-level cone of depression occurs in the distal fan area. Nonetheless, the calculated subsidence bowl closely approximates the observed one located much farther inland. Without requiring extensive calibration or an elaborate numerical groundwater flow and subsidence model, the model provides reasonable and detailed patterns using a spatially varying relationship between drawdown and resulting land subsidence. Results indicate that the spatial regression model reasonably estimates the spatial distribution of the skeletal storage coefficient in the aquifer system. The large coefficient that represents inelastic compaction occurs in the inland areas, whereas the small coefficient that represents elastic compaction occurs along the coastal area. Furthermore, this model is relevant for water policy or land subsidence regulation.

Introduction

Land subsidence caused by excessive groundwater exploitation is a severe problem in numerous cities and regions, including Shanghai (Shen and Xu, 2011; Xu et al., 2016), Mexico City (Kirwan and Megonigal, 2013), Bangkok (Phien-Wej et al., 2006), Iran (Amiraslani and Dragovich, 2011; Rahmati et al., 2019), Las Vegas (Bell et al., 2008; Hoffmann et al., 2001) and the San Joaquin Valley in California (Faunt et al., 2016; Poland, 1972). These areas with problematic subsidence have long been monitored; their distribution and extent of subsidence and water-level decline are well established as the result of the compaction of fine-grained aquitards and interbeds due to aquifer overexploitation (Bonì et al., 2016). The removal of water from storage in fine-grained silts and clays, interbedded within the aquifer system, causes these highly compressible sediments to compact and cause land subsidence. Furthermore, large-scale groundwater utilization from human activities causes environmental problems (Rahmati et al., 2019), such as land degradation, soil salinization and desertification.

Land subsidence is correlated with variations of the aquifer system pore pressures or water-level response to pumping (Burbey, 2001). The drawdown of water levels leads to land subsidence from over-extraction of groundwater (Bell et al., 2008; Galloway and Burbey, 2011). However, generating the subsidence–drawdown

relation is critical to better understand and predict the spatial distribution of land subsidence. Accurate modeling requires observations of land deformation and water levels over months to years of time (Faunt et al., 2016; Kim, 2000; Yan and Burbey, 2008). To model the subsidence–drawdown relation, traditional numerical groundwater flow models such as MODFLOW (Mahmoudpour et al., 2016; Shearer, 1998; Zhou et al., 2003) combined with a post-processing software package such as GMS (Parhizkar et al., 2015) can provide water-level and flow distributions of the system under observation. Thus, land subsidence can be simulated from changes in water pressure within the aquifer system coupled with the SUB Package (Hoffmann et al., 2003b). A coupled numerical model that incorporates the concepts of three dimensional poroelasticity based on Biot's consolidation theory (Biot, 1941, 1955) is developed for simulating three dimensional displacement of solids within unconsolidated aquifers in response to induced changes in water pressure (Burbey, 2006; Burbey and Helm, 1999). Elastic (recoverable) and inelastic (permanent) compaction from stress–strain diagrams (Epstein, 1987; Hanson, 1989; Riley, 1969) can be identified. Fine-grained sediments tend to compact inelastically if the effective stress exceeds the preconsolidation stress. Decreasing hydraulic heads, such as by increasing effective stresses, causes a small amount of elastic compaction if the effective stress remains less than the preconsolidation stress (Galloway and Burbey, 2011). However, uncertainty still exists in traditional numerical models because heterogeneous geological conditions cannot be described in the same detail that occurs in nature.

Reasonable estimates of the subsidence–drawdown relation can be obtained from regression models using land subsidence and drawdown data, provided sufficient subsidence data and water-level records are available for the area of investigation (Yan and Burbey, 2008). However, drawdown and subsequent compaction of compressible hydrogeologic layers can result in spatially non-uniform and heterogeneous land subsidence of the hydrogeological system (Galloway et al., 1998a; Hoffmann et al., 2003a; Teatini et al., 2006). The subsidence–drawdown relation is rarely well correlated and therefore seldom readily applied in multi-linear regression analyses (Jiang et al., 2015). Moreover, the subsidence–drawdown function is found to be far more heterogenous than most previous studies suggest (Sundell et al., 2019). Spatial regression (SR), i.e. geographically weighted regression (GWR), is a local form of linear regression used to model spatially varying relationships (Fotheringham, et al., 2003). Such methods are powerful for capturing the effects of spatially heterogeneous processes and can identify spatial nonstationarity in the subsidence–drawdown relation by allowing regression coefficients to vary spatially. However, previous studies on SR merely consider the relationship between subsidence and groundwater level variation at starting and ending times without considering any compaction processes (Shang et al., 2011).

The present study aims to estimate the spatially variable land subsidence distribution based on accumulated drawdown between ground-based observations and to improve the limitations of linear regression methods, which typically fail in spatial hydrogeologic settings. The SR-based method developed in this study provides a reliable model of the spatial relationship between accumulated drawdown and the resulting land subsidence. The model coefficients are expected to provide the spatial patterns of elastic and inelastic storage coefficients of the aquifer. In addition, a spatial subsidence map is proposed based on only the groundwater drawdown distributions in the aquifer system.

Study area and data

Study area

The Choshui River alluvial fan is located in the mid-western coast of Taiwan and includes the counties of Changhua and Yunlin. The Choshui River runs from east to west through the study area (Fig. 1a), which covers approximately 1800 km^2, and bisects the two counties. The alluvial plain is surrounded by natural geographical boundaries that include the Taiwan Strait to the west, the Central Mountain Ridge to the east, the Wu River to the north, and the Beigang River to the south (Yu and Chu, 2010). The measured groundwater levels of the aquifers indicate that the system has two major flow directions, one from the eastern mountain area to the northwest in Changhua and the other in a southwest direction in Yunlin.

Fig. 2 shows a hydrogeological profile of the Choshui River alluvial fan that comprises Aquifers I, II-1, II-2,

III, and IV (F1–F4 in Fig. 2) measured from the land surface downward. Aquitards (T1–T3) separate the aquifers. Aquitards are most relevant in the distal-fan and mid-fan areas and gradually diminish in thickness toward the east. The proximal-fan represents the major recharge area of the aquifer system (Jang et al., 2008; Yu and Chu, 2010).The distribution of sediments in the alluvial fan transitions from largely gravel, to sand, and then to clay from the proximal fan to the distal fan. Moreover, Aquifer II is the major aquifer of the Choshui alluvial plain because of its large spatial extent and acceptable depth for groundwater extraction (Liu et al., 2004; Yu and Chu, 2010).

Given the insufficient surface water supply in the alluvial fan, residents extract groundwater to supplement their demands for irrigation, aquaculture, and household domestic use, especially in dry seasons. Groundwater is the major source of water for civilian and agricultural use and represents approximately 240,000 m^3/day in the study area. The majority of water is used in agriculture, such as rice paddies, with 1.8 and 1.5 billion cubic meters per year on average for Changhua and Yunlin, respectively (Lee et al., 2018). Groundwater overdraft causes serious land subsidence in the area, especially during droughts. An area of approximately 300 km^2 experiences significant subsidence ($>$ 3 cm/year in 2015), despite the enforced restrictions on groundwater exploitation. Fig. 1b shows spatial pattern of observed land subsidence.

Required data for this investigation

This investigation uses monthly groundwater level observations in 2015. The water-level observations of aquifer layers 1, 2, 3, and 4 obtained from 33, 40, 28, and 28 monitoring wells, respectively, are evenly distributed over the entire Choshui River alluvial fan (Fig. 1a).

In addition, annual subsidence rates for 2015 from 662 leveling points (Fig. 1a) have been collected. A leveling network amounting to over 1,000 km in length is used to calculate subsidence for every 1.5 km interval along the leveling routes. Leveling specifications satisfy a loop closure of less than $3\sqrt{K}$ mm, where K is the length of the leveling circuit in kilometers. The vertical accuracy of leveling data is generally within 1 cm (Hung et al., 2010). Leveling has a high degree of accuracy but is time consuming and expensive compared with GPS. The leveling and groundwater level data are obtained from the Water Resources Agency of Taiwan.

Data Analysis Methods

Model development

Based on Terzaghi's principle of effective-stress (Hoffmann et al., 2003a), the nonlinear stress–compaction relation is typically linearized with respect to preconsolidation stress (Shen and Xu, 2011). The calculation of total aquifer system compaction (subsidence) can be linearized where incremental changes in effective stress (hydraulic head) are typically small, as

$\Delta z = S_k \Delta h$, (1)

where Δz is the subsidence, S_k is the skeletal storage coefficient, and h is the change in hydraulic head. If the effective stress remains less than the preconsolidation stress (or less than the past maximum drawdown), the compaction is entirely elastic. In this study, the soil rebound (volume expansion after removal of mechanical stress) is disregarded from h, which represents the annual cumulative drawdown or the total annual change in hydraulic head (Chu and Chang, 2009). Rebound tends to be less than 10% of the original subsidence (Chaussard et al., 2014a). The total annual drawdown is then stated as:

$\Delta h = \sum_t h_t$, (2)

where $h_t = h_{t+1} - h_t$ if . In this one-year case, the time step t varies from 1–12 representing the months of the year.

Subsidence is a function of accumulated drawdown. Furthermore, a regression expression identifies the relation between subsidence and groundwater level. Equation (1) is extended to yield an estimate of subsidence at observation i in a multi-layer aquifer, which can be expressed as:

$z_i = \sum_l S_{\mathrm{kl}} h_{\mathrm{il}} + \varepsilon_i$, (3)

where l is the layer number in the multi-layer aquifer,S_{kl} is the l th skeletal storage coefficient in a multi-layer system and z_i is the land subsidence at observation$i$. This study uses the annual subsidence rate for 2015 and h_{il} is the estimated total groundwater decline (drawdown) at observation i from aquifer layer l .ε_i is the residual of the regression model. Equation (3) is further extended to allow for spatially varying subsidence and drawdown in a multi-layer aquifer system as follows:

$z_i = \sum_l S_{\mathrm{kl}}(u_i, v_i) h_{\mathrm{il}} + \beta_0(u_i, v_i) + \varepsilon_i$, (4)

where $S_{\mathrm{kl}}(u_i, v_i)$ varies with the spatial coordinates (u_i, v_i) at observation i and is the slope of the spatial regression parameters in the l th layer.$\beta_0(u_i, v_i)$ is the intercept at observation$i$ of the spatial regression parameters in the multi-layer system. The slope coefficient in Equation (4) without the interceptβ_0 represents the skeletal storage coefficient S_k in each aquifer, which is required to accurately estimate subsidence from drawdown.

Spatial coefficient estimation

The SR is an extension of ordinary least squares (OLS) (Fotheringham et al., 2003). Using the SR, the estimated parameter matrix$\hat{\beta}(u_i, v_i)$, which includes$S_{\mathrm{skl}}(u_i, v_i)$ at each observation$i$ is expressed as:

$\hat{\beta}(u_i, v_i) = [H^T W(u_i, v_i) H]^{-1} H^T W(u_i, v_i) Z$, (5)

where

$H =$

$$\begin{bmatrix} 1 & amp;h_{11}\cdots & amp;h_{1L} \\ \vdots & amp;\ddots & amp;\vdots \\ 1 & amp;h_{n1}\cdots & amp;h_{\mathrm{nL}} \end{bmatrix}, Z =$$

$$\begin{bmatrix} z_1 \\ \vdots \\ z_n \end{bmatrix}, \quad (6)$$

$W(u_i, v_i) = diag(w_1(i), \ldots w_j(i) \ldots, w_n(i))$, and (7)

$\hat{\beta}(u_i, v_i) = (\beta_0(u_i, v_i), S_{k1}(u_i, v_i), \ldots, S_{\mathrm{kL}}(u_i, v_i))^T$. (8)

H and Z represent the matrix form of h_{il} andz_i for the n observations and L layers used in this study. $W(u_i, v_i)$ is a spatial weight matrix based on the Euclidean and Gaussian distance decay-based functions in the spatial domain. In this case, the Euclidean distance is expressed in meters. The parameter $w_j(i)$ between observations$i$ and neighboring j in the spatial weight matrix is commonly used as a kernel and represents a Gaussian distance decay-based function,$w_j(i) = exp\left(-\frac{D_{\mathrm{ij}}^2}{b^2}\right)$, where D_{ij} is the Euclidian distance between observations$i$ and j .$D_{\mathrm{ij}} = \sqrt{(u_i - u_j)^2 + (v_i - v_j)^2}$and b is the non-negative parameter known as the bandwidth (Brunsdon et al., 1996; Chu et al., 2018). Bandwidth b can be determined by several criteria, such as the cross validation (CV) procedure (Fotheringham et al., 2003). The CV procedure is used to select the optimal parameters b :

$\mathrm{CV}(b) = \sum_i (\Delta\zeta_i - \Delta\zeta_{\neq i}(b))^2$. (9)

For comparison, the models for linear and spatial regressions i.e., OLS and SR are applied on all four aquifer layers, including mixed and single layer drawdowns from different aquifers. Spatial estimation of the drawdown is applied using inverse distance weighting (IDW). The models are developed using MATLAB. Model 1 is based on the cumulative drawdown from all aquifer layers. Models 2–5 are based on only drawdowns from Layers 1–4 without the y-intercept, respectively, as shown at a later stage.

To evaluate the model performance, the common measures R^2 and RMSEs are used on the basis of observation data and estimated values at these points.

Results and discussion

The subsidence–accumulated drawdown relation was built in linear and spatial regressions; that is, the SR model. First, a relation between total subsidence and multi-layer drawdowns was accurately formulated, and the spatial patterns of subsidence were subsequently estimated.

Overview of subsidence and drawdown

Fig. 3 displays the correlation between subsidence and variations in groundwater level. The subsidence–drawdown relation is nonlinear (correlation coefficient = 0.27, 0.54, 0.57, and 0.54, respectively, in each of the four aquifer layers). Groundwater drawdowns in Layers 2–4 are similar (correlation coefficient = 0.84 in Layers 2 and 3; 0.78 in Layers 2 and 4). Drawdowns in Layer 1 (unconfined aquifer) vary spatially over shorter distances compared to those of the confined aquifer (Layers 2–4). Figs. 1b and 4 show the spatial distribution of annual observed subsidence and accumulated drawdown, respectively, for 2015, when the maximum annual permanent subsidence is approximately 7 cm (Fig. 1b). The spatial distribution of subsidence reveals a bowl in the central area of Yunlin (Hwang et al., 2008). Within the study area, the maximum accumulated drawdown in Layers 1–4 ranges from 15–20 m (Fig. 4). The cumulative drawdowns implies that similar cones of depression are located in Layers 2–4 in the southwest distal fan area, near the coast. Drawdown cones are located along the distal fan and mountain areas in Layer 1. Compared with the four-layer drawdown pattern, the drawdown is greatest in Layer 2 in the study area. In addition, drawdowns in Layers 2–4 are highly correlated (Fig. 3), while Layer 3 is most closely correlated to the subsidence of the four-layer drawdown model (Fig. 3).

The compression behavior of clay agrees with Terzaghi's consolidation theory (Liu et al., 2004). Land subsidence with inelastic compression continues as water levels continuously decline. The inelastic compression of fine-grained aquifer interbeds is likely responsible for the vast majority of subsidence problems, based on the compressibility and total thickness of fine-grained deposits throughout the region (Galloway et al., 1998b; Galloway and Sneed, 2013). The cone of maximum drawdown occurs in the distal fan area, whereas the current major subsidence bowl occurs inland. Consequently, the cone of maximum drawdown fails to fully coincide with the location of the subsidence bowl (Erban et al., 2014). In the coastal area or distal fan area, the rate of pumping is proposed to decrease to stabilize or reduce water level declines. This subsequently reduces land subsidence, given that the largest occurrence in the inland area induced by heavy withdrawal of groundwater. This is a sensitive environmental concern because the Taiwan High Speed Rail is constructed through the central subsidence area, which might pose a serious threat to its operation (Hwang et al., 2008; Tung and Hu, 2012).

Model performance

The performance of SR such as the RMSEs in the multi- or single-aquifer system (RMSE = 0.6–0.8 cm) is better than that of OLS (RMSE = 1.58–2.11 cm) (Table 1). The best models are appear to be Model 1 in the multi-aquifer system and Model 4 in the single-aquifer system. However, the subsidence–drawdown model using OLS is not appropriate due to its poor performance (Table 1). The SR is more accurate than that of OLS. Results of OLS reveal a subsidence–drawdown function with negative a slope for Layer 1 (high drawdown -low subsidence exists in the proximal fan) but a positive slope for Layers 2, 3, and 4 in Model 1 (Table 2). Compared with Models 2–5, the best SR with the lowest RMSEs occurs in Model 4 because the subsidence–drawdown correlation is the highest, but the poorest model with highest RMSE is Model 2 due to its low subsidence–drawdown correlation (Fig. 3). Considering the validation using the GPS data of ground surface (Fig 1), the RMSEs of Model 4 using linear regression and SR are 1.52 and 0.67 cm, respectively. Validation of our subsidence model with available GPS data provides consistent and accurate results.

Fig. 5 shows the total estimated land subsidence calculated from linear regression and SR using all-layers

(Model 1) and single layer drawdowns (Models 2–5). In a linear regression, the estimated land subsidence bowl occurs in the distal fan area (near the coast), but also in the proximal and distal fan areas in Model 2 due to the variable drawdown patterns occurring in Layer 1. The estimated maximum subsidence in the OLS models occurs at the boundary area of Yunlin, whereas in the SR models subsidence occurs in the inland area of Yunlin (Fig. 5). However, the estimated pattern using OLS does not match the observed subsidence. The SR explicitly considers spatially dependent models to overcome the spatial variability of land subsidence mapping because the SR extends the linear regression by estimating a set of spatial parameters rather than one single set of parameters (Brunsdon et al., 1996; Fotheringham et al., 2003). The model RMSEs are less than or equal to 0.8 cm so that the spatial regression can be used to model spatially varying relationships between subsidence and drawdown in the aquifer system.

Spatial model coefficient and implication

Fig. 6 exhibits the spatial pattern of regression slope coefficients of the SR in Layers 1–4 for Models 2–5. The regression coefficient distribution varies spatially. The patterns of spatial coefficients are typically similar in Layers 2, 3, and 4. Most coefficients have a positive slope for total drawdown and subsidence (Fig. 6). Only the proximal fan and the area close to Wu River exhibits a negative relation between the total drawdown and land subsidence (Fig. 6). A negative relation can occur where unloading causes a small soil rebound or where drawdown continues but the subsidence rate declines due to recharge effects (i.e., rainfall, ponds/lakes, canals, and irrigation).

The long-term trend of hydraulic head and vertical displacements are useful to estimate the inelastic skeletal storage coefficient for subsidence features (Miller and Shirzaei, 2015). The spatial patterns of skeletal storage coefficients in four layers can be estimated using the slope coefficients of spatial regression (Fig. 6), which also reflect the skeletal storage coefficients of the aquifers. In Fig. 6(c), the large coefficient value (purple color) represents inelastic compaction in the inland area, whereas the small coefficient value (blue color) represents elastic compaction in other areas. The resulting subsidence pattern clearly suggests elasto-plastic mechanical behavior, which includes elastic and inelastic skeletal storage in over-consolidated and normally consolidated soils (Hung et al., 2012; Liu et al., 2004). In recent decades, the excessive pumping of groundwater has resulted in serious subsidence problems along the coast. This subsidence coincides with the increase of aquaculture fisheries since the 1970s. Currently, the rate of compaction in the coastal area is declining. However, the subsidence bowl is moving inland due to over-pumping in this region (Hwang et al., 2008). Interferometric Synthetic Aperture Radar (InSAR) offers a powerful and useful method for identifying regional land subsidence (Bürgmann et al., 2000; Bonì et al., 2016; Chaussard et al., 2014b; Galloway et al., 1998b; Hoffmann et al., 2001). The present findings match the results from previous InSAR interferograms for the study region (Tung and Hu, 2012). Moreover, the advent and use of GPS has made land subsidence monitoring more efficient and cost effective. However, GPS is limited because it measures only the surface deformation at point locations (Hosseini et al., 2007). The approach developed in the present study provides robust and accurate maps of estimated land subsidence that are far more spatially descriptive than those that GPS typically provides.

In the developed models, spatial patterns of subsidence are estimated solely on the basis of drawdown information. The effect of groundwater-level changes on land subsidence can be modeled using a stress–strain relationship with the elastic or inelastic skeletal storage coefficient of the underlying aquifers. However, the entire system includes leveling surveys, borehole extensometer data, and multilayer monitoring of groundwater levels, with the aim to better understand the hydrological and mechanical processes of the aquifer system and to characterize the spatial distribution of land subsidence with a traditional numerical model (Zhang et al., 2014). Characterizing the hydrogeological setting of the aquifer system is a critical step to accomplish this goal (Liu et al., 2004). The observational data used to characterize hydrogeology is limited (Hubbard and Rubin, 2000) including the hydraulic diffusivity of the confining layer, the distance from the pumping wells, length of the recovery cycle, and the thickness of confining layers. All of these factors can influence the shape of stress–strain hysteresis loops (Burbey, 2001).

In this study, further calibration of the model is not required, unlike other numerical models that typically

require an inverse modeling component for calibration purposes. The fundamental benefit of inverse modeling is its ability to automatically estimate parameter values that produce the best fit between observed and simulated hydraulic heads and flows (Franssen et al., 2009; Poeter and Hill, 1997). However, limitations include model uncertainty (hydrogeologic characterization of the system), and measurement and parameter uncertainties (Højberg and Refsgaard, 2005). For example, the numerical model contains parameter uncertainty due to the unknown pumping rates, which can limit the ability to adequately characterize key hydrologic parameters. Therefore, this method can be used efficiently for subsidence management and might be widely used for subsidence prediction solely based on drawdown. Subsidence is influenced by drawdown due to persistent pumping and effects of dry–wet cycles and seasonal variations of groundwater levels (Kouda et al., 2015). This subsidence–drawdown model can be relevant in terms of policy or land subsidence regulation.

Conclusions

This study implements a spatial regression-based subsidence-mapping scheme on the basis of groundwater-level observations and offers an effective method to explore the spatial patterns of subsidence through its correlation with drawdowns, without the use of complex hydrogeologic models. The model developed here is based on a SR method and is easy to fit between the total drawdown and subsidence observations. A goodness-of-fit better than OLS (RMSEs are less than or equal to 0.8 cm) is achieved. Without requiring a more detailed hydrogeologic investigation and extensive calibration, this model offers reasonable detail regarding the spatial patterns of land subsidence using a non-linear and spatially varying relationship between the water-level observations and resulting land subsidence. This model can be relevant for water resource policy or land subsidence regulation.

The developed model accurately estimates the spatial pattern of land subsidence. The estimated subsidence bowl occurs in the inland area of Yunlin, similar to the actual observed subsidence bowl location. However, the drawdown cone occurs in the coastal area west of the subsidence bowl. The model can estimate the spatial pattern of subsidence that is highly related to the hydrogeological properties and drawdown history, which impacts the location of the observed subsidence bowl. Results also show that the model coefficients accurately reflect the skeletal storage coefficients of the aquifer. The large coefficient value represents inelastic compaction in the inland area, whereas the small coefficient value represents the elastic compaction that occurs along the coastal area. The coefficient patterns represent elastic and inelastic skeletal storage coefficients in over-consolidated and normally consolidated soils.

In a future study, the recharge effects and hydrodynamic lag that exists between the drawdown and subsequent subsidence can be considered. The prediction of long-term subsidence or subsidence time series can then be investigated.

Data Availability Statement

The data that support the findings of this study are available from Water Resources Agency of Taiwan. Restrictions apply to the availability of these data, which were used under license for this study. Data are available from Chu et al. with the permission of Water Resources Agency of Taiwan.

Acknowledgements

The authors thank the MOST for their financial support (105-2621-M-006-011-).

Table 1. Model performance comparison for OLS and SR (Model 1: Layers 1–4; Models 2: Layer 1; Models 3: Layer 2; Models 4: Layer 3; (e) Models 5: Layer 4)

	R^2 in OLS	R^2 in SR	RMSE (cm) in OLS	RMSE (cm) in SR
Model 1	0.42	0.98	1.58	0.60
Model 2	0.31	0.97	2.11	0.79
Model 3	0.31	0.97	1.73	0.75
Model 4	0.37	0.98	1.64	0.67

	R^2 in OLS	R^2 in SR	RMSE (cm) in OLS	RMSE (cm) in SR
Model 5	0.33	0.97	1.66	0.73

Table 2. Model coefficients, namely, slopes for OLS and SR (Model 1: Layers 1–4; Models 2: Layer 1; Models 3: Layer 2; Models 4: Layer 3; (e) Models 5: Layer 4)

	Slope in OLS	Average Slope in SR
Model 1	-0.316* (Layer1) 0.114* (Layer2) 0.492* (Layer3) 0.130* (Layer4)	-0.204 (Layer1) 0.172 (Layer2) 0.372 (Layer3) 0.070 (Layer4)
Model 2	0.813* (Layer1)	0.880 (Layer1)
Model 3	0.530* (Layer2)	0.520 (Layer2)
Model 4	0.526* (Layer3)	0.476 (Layer3)
Model 5	0.650* (Layer4)	0.675 (Layer4)

Note: *Coefficient in OLS is statistically significant with p-value < 0.05

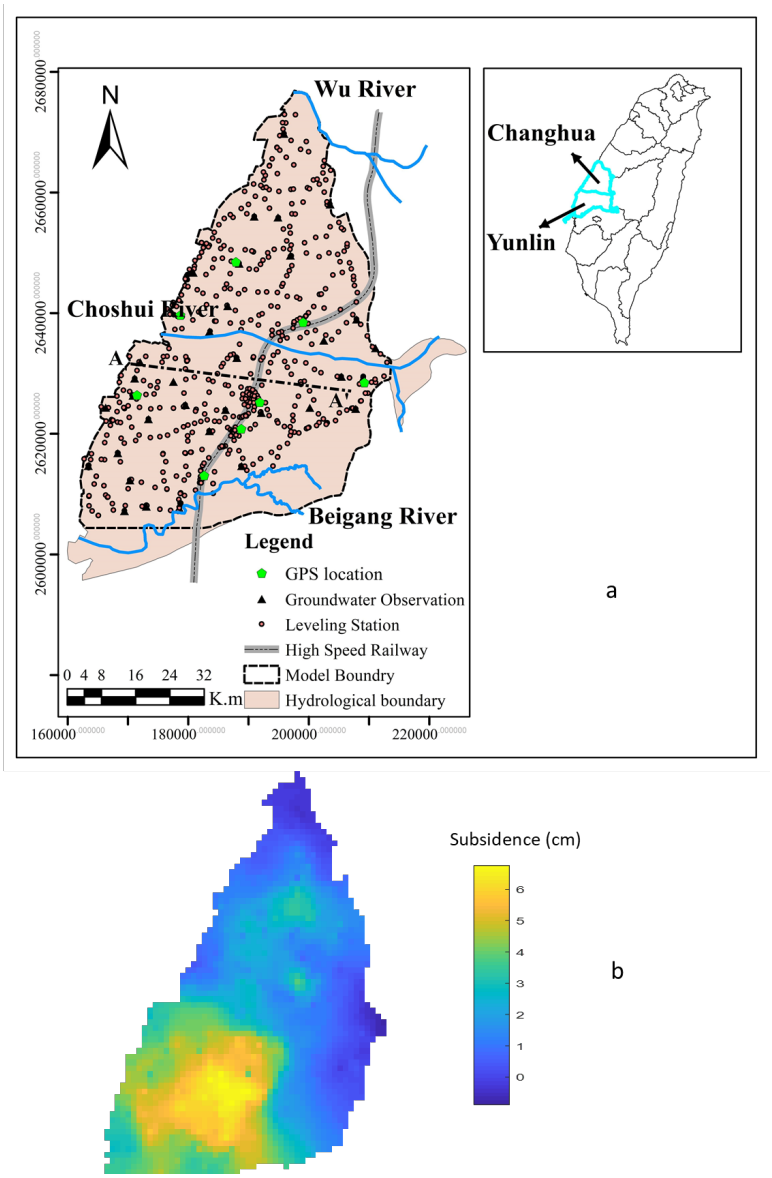

Fig. 1(a). Map showing the location of the study area and observation network, which includes leveling stations (orange circle) and water table observations (black triangle); (b) Observed and interpolated subsidence for 2015 (unit: cm). IDW interpolation is based on leveling data.

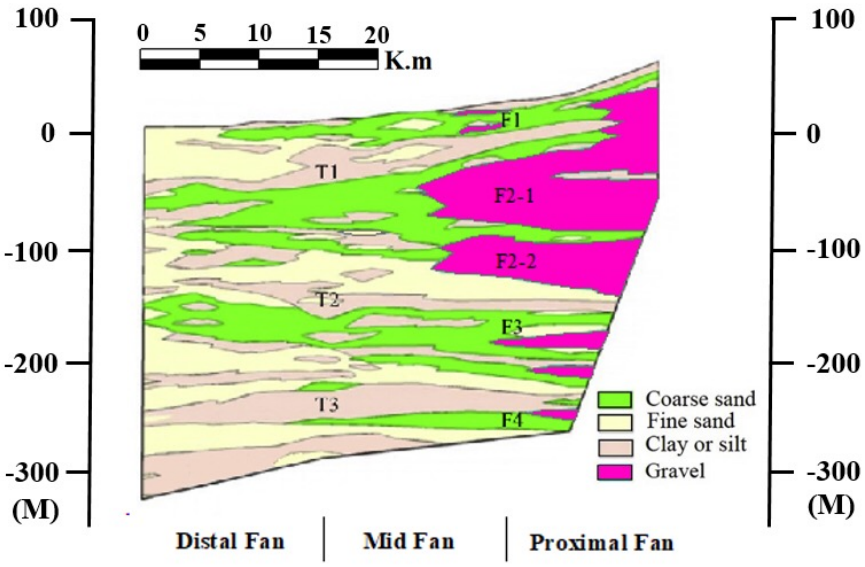

Fig. 2. Hydrogeological profile in the Choshui River alluvial fan in an east–west direction, A–A' (Central Geological Survey, 1999)

Hosted file

`image4.emf` available at https://authorea.com/users/311669/articles/442372-development-of-a-groundwater-drawdown-function-to-estimate-spatially-varying-land-subsidence-a-case-study-of-the-choshui-river-basin-taiwan

Fig. 3. Correlations between subsidence (z) and groundwater level variations, such as cumulative drawdowns in the four aquifer layers (h1–h4)

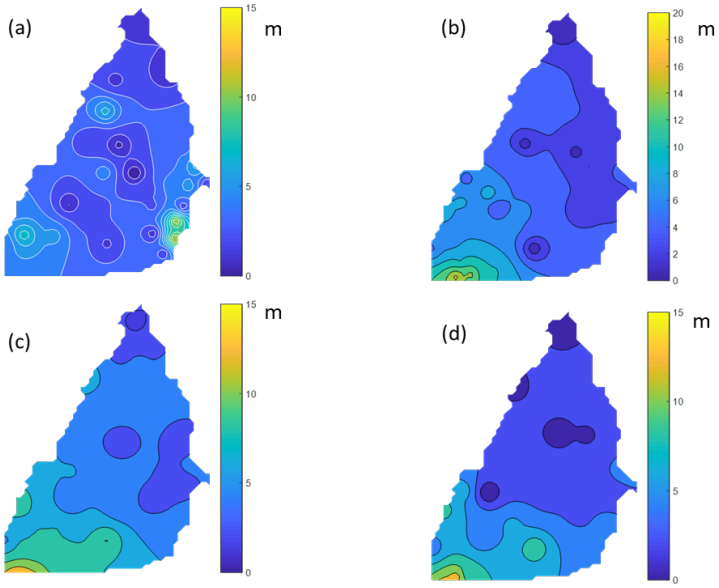

Fig. 4. Annual accumulated groundwater level declines (m) in 2015 in aquifer Layers 1–4 (a–d)

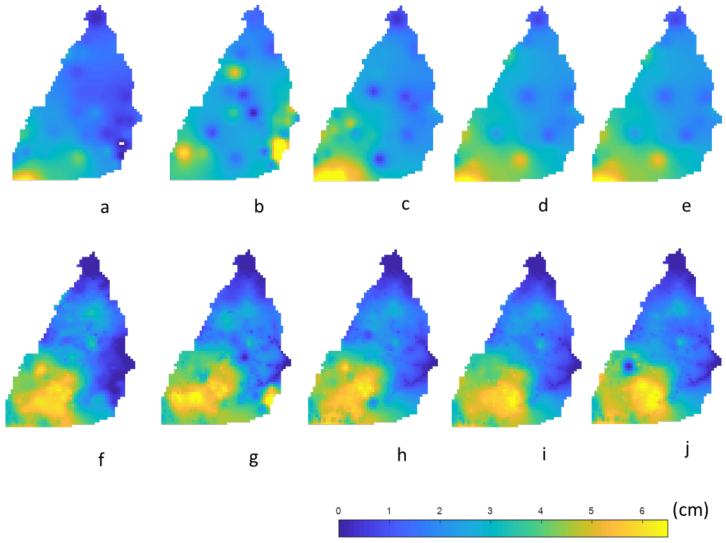

Fig. 5. Estimated land subsidence (cm) (a) Layers 1–4; (b) Layer 1; (c) Layer 2; (d) Layer 3; (e) Layer 4 for OLS; and (f) Layers 1–4; (g) Layer 1; (h) Layer 2; (i) Layer 3; and (j) Layer 4 for SR

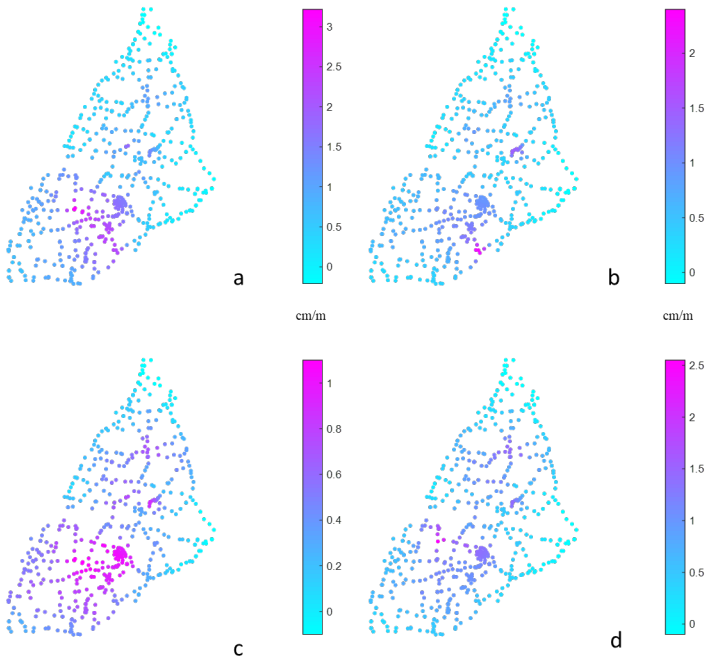

Fig. 6. Slope coefficients of SR (cm/m) for (a) Layer 1 in Model 2; (b) Layer 2 in Model 3; (c) Layer 3 in Model 4; and (d) Layer 4 in Model 5

References

Amiraslani, F., Dragovich, D., 2011. Combating desertification in Iran over the last 50 years: an overview of changing approaches. J. Environ. Manage. 92, 1-13.

Bürgmann, R., Rosen, P.A., Fielding, E.J., 2000. Synthetic aperture radar interferometry to measure Earth's surface topography and its deformation. Ann. Rev. Earth Planet. Sci. 28, 169-209.

Bell, J.W., Amelung, F., Ferretti, A., Bianchi, M., Novali, F., 2008. Permanent scatterer InSAR reveals seasonal and long-term aquifer-system response to groundwater pumping and artificial recharge. Water Resour. Res. 44.

Biot, M.A., 1941. General theory of three-dimensional consolidation. J. Appl. Phys. 12, 155-164.

Biot, M.A., 1955. Theory of elasticity and consolidation for a porous anisotropic solid. J. Appl. Phys. 26, 182-185.

Bonì, R., Cigna, F., Bricker, S., Meisina, C., McCormack, H., 2016. Characterisation of hydraulic head changes and aquifer properties in the London Basin using Persistent Scatterer Interferometry ground motion data. J. Hydrol. 540, 835-849.

Brunsdon, C., Fotheringham, A.S., Charlton, M.E., 1996. Geographically weighted regression: a method for exploring spatial nonstationarity. Geogr. Anal. 28, 281-298.

Burbey, T.J., 2001. Stress-strain analyses for aquifer-system characterization. Groundwater 39, 128-136.

Burbey, T.J., 2006. Three-dimensional deformation and strain induced by municipal pumping, Part 2: Numerical analysis. J. Hydrol. 330, 422-434.

Burbey, T.J., Helm, D.C., 1999. Modeling three-dimensional deformation in response to pumping of unconsolidated aquifers. Environ Eng Geosci., 199-212.

Chaussard, E., Burgmann, R., Shirzaei, M., Fielding, E., Baker, B., 2014a. Predictability of hydraulic head changes and characterization of aquifer-system and fault properties from InSAR-derived ground deformation. J. Geophys. Res. Solid Earth 119, 6572-6590.

Chaussard, E., Wdowinski, S., Cabral-Cano, E., Amelung, F., 2014b. Land subsidence in central Mexico detected by ALOS InSAR time-series. Remote Sens. Environ. 140, 94-106.

Chu, H.-J., Chang, L.-C., 2009. Optimizing capacity-expansion planning of groundwater supply system between cost and subsidence. J. Hydrol. Eng. 15, 632-641.

Chu, H.-J., Kong, S.-J., Chang, C.-H., 2018. Spatio-temporal water quality mapping from satellite images using geographically and temporally weighted regression. Int. J. Appl. Earth Obs. 65, 1-11.

Epstein, V.J., 1987. Hydrologic and geologic factors affecting land subsidence near Eloy, Arizona. Water -Resources Investigations Report 87-4143, 28.

Erban, L.E., Gorelick, S.M., Zebker, H.A., 2014. Groundwater extraction, land subsidence, and sea-level rise in the Mekong Delta, Vietnam. Environ. Res. Lett. 9, 084010.

Faunt, C.C., Sneed, M., Traum, J., Brandt, J.T., 2016. Water availability and land subsidence in the Central Valley, California, USA. Hydrogeol. J. 24, 675-684.

Fotheringham, A.S., Brunsdon, C., Charlton, M., 2003. Geographically weighted regression: the analysis of spatially varying relationships. John Wiley & Sons.

Franssen, H.H., Alcolea, A., Riva, M., Bakr, M., Van der Wiel, N., Stauffer, F., Guadagnini, A., 2009. A comparison of seven methods for the inverse modelling of groundwater flow. Application to the characterisation of well catchments. Adv. Water Resour. 32, 851-872.

Galloway, D.L., Burbey, T.J., 2011. Review: Regional land subsidence accompanying groundwater extraction. Hydrogeol. J. 19, 1459-1486.

Galloway, D.L., Hednut, K.W., Ingebritsen, S.E., Phillips, S.P., Peltzer, G., Rogez, F., Rosen, P.A., 1998a. InSAR detection of system compaction and land subsidence, Antelope Valley, Mohave Desert, California. Water Resour. Res. 34, 2573-2585.

Galloway, D.L., Hudnut, K.W., Ingebritsen, S., Phillips, S.P., Peltzer, G., Rogez, F., Rosen, P., 1998b. Detection of aquifer system compaction and land subsidence using interferometric synthetic aperture radar, Antelope Valley, Mojave Desert, California. Water Resour. Res. 34, 2573-2585.

Galloway, D.L., Sneed, M., 2013. Analysis and simulation of regional subsidence accompanying groundwater abstraction and compaction of susceptible aquifer systems in the USA. Boletin de la Sociedad Geologica Mexicana 65, 123-136.

Hojberg, A., Refsgaard, J., 2005. Model uncertainty–parameter uncertainty versus conceptual models. Water Sci. Technol. 52, 177-186.

Hanson, R.T., 1989. Aquifer-system compaction, Tucson Basin and Avra Valley, Arizona. U.S. Geological Survey.

Hoffmann, J., Galloway, D.L., Zebker, H.A., 2003a. Inverse modeling of interbed storage parameters using land subsidence observations, Antelope Valley, California. Water Resour. Res. 39, SBH 5-1 to 5-13.

Hoffmann, J., Leake, S.A., Galloway, D.L., Wilson, A.M., 2003b. MODFLOW-2000 ground-water model–User guide to the subsidence and aquifer-system compaction (SUB) package. Geological Survey Washington DC.

Hoffmann, J., Zebker, H.A., Galloway, D.L., Amelung, F., 2001. Seasonal subsidence and rebound in Las Vegas Valley, Nevada, observed by synthetic aperture radar interferometry. Water Resour. Res. 37, 1551-1566.

Hosseini, M., Zoej, M.V., Mobasheri, M., Dehghani, M., 2007. Land subsidence monitoring using InSAR and GPS. Map Asia.

Hubbard, S.S., Rubin, Y., 2000. Hydrogeological parameter estimation using geophysical data: a review of selected techniques. J. Contam. Hydrol. 45, 3-34.

Hung, W.-C., Hwang, C., Chang, C.-P., Yen, J.-Y., Liu, C.-H., Yang, W.-H., 2010. Monitoring severe aquifer-system compaction and land subsidence in Taiwan using multiple sensors: Yunlin, the southern Choushui River Alluvial Fan. Environmental Earth Sciences 59, 1535-1548.

Hung, W.-C., Hwang, C., Liou, J.-C., Lin, Y.-S., Yang, H.-L., 2012. Modeling aquifer-system compaction and predicting land subsidence in central Taiwan. Eng. Geol. 147, 78-90.

Hwang, C., Hung, W.-C., Liu, C.-H., 2008. Results of geodetic and geotechnical monitoring of subsidence for Taiwan High Speed Rail operation. Nat. Hazards 47, 1-16.

Jang, C.S., Chen, S.K., Ching-Chieh, L., 2008. Using multiple-variable indicator kriging to assess groundwater quality for irrigation in the aquifers of the Choushui River alluvial fan. Hydrol. Process. 22, 4477-4489.

Jiang, Y., Liu, J.-R., Luo, Y., Yang, Y., Tian, F., Lei, K.-C., 2015. Research on critical groundwater level under the threshold value of land subsidence in the typical region of Beijing. Proceedings of the International Association of Hydrological Sciences 372, 507-510.

Kim, J.-M., 2000. Generalized poroelastic analytical solutions for pore water pressure change and land subsidence due to surface loading. Geosci. J. 4, 95.

Kirwan, M.L., Megonigal, J.P., 2013. Tidal wetland stability in the face of human impacts and sea-level rise. Nature 504, 53.

Kouda, A., Nagata, K., Sato, T., 2015. Factor analysis on land subsidence in the Nobi Plain, southwest Japan. Proceedings of the International Association of Hydrological Sciences 372, 95-99.

Lee, M., Yu, C.-Y., Chiang, P.-C., Hou, C.-H., 2018. Water–Energy Nexus for Multi-Criteria Decision Making in Water Resource Management: A Case Study of Choshui River Basin in Taiwan. Water 10, 1740.

Liu, C.-H., Pan, Y.-W., Liao, J.-J., Huang, C.-T., Ouyang, S., 2004. Characterization of land subsidence in the Choshui River alluvial fan, Taiwan. Environ. Geol. 45, 1154-1166.

Mahmoudpour, M., Khamehchiyan, M., Nikudel, M.R., Ghassemi, M.R., 2016. Numerical simulation and prediction of regional land subsidence caused by groundwater exploitation in the southwest plain of Tehran, Iran. Eng. Geol. 201, 6-28.

Miller, M.M., Shirzaei, M., 2015. Spatiotemporal characterization of land subsidence and uplift in Phoenix using InSAR time series and wavelet transforms. J. Geophys. Res. Solid Earth 120, 5822-5842.

Parhizkar, S., Ajdari, K., Kazemi, G.A., Emamgholizadeh, S., 2015. Predicting water level drawdown and assessment of land subsidence in Damghan aquifer by combining GMS and GEP models. Geopersia 5, 63-80.

Phien-Wej, N., Giao, P., Nutalaya, P., 2006. Land subsidence in bangkok, Thailand. Eng. Geol. 82, 187-201.

Poeter, E.P., Hill, M.C., 1997. Inverse models: A necessary next step in ground-water modeling. Groundwater 35, 250-260.

Poland, J.F., 1972. Land subsidence in the western states due to ground-water overdraft. Water Resour. Bull. 8, 118-131.

Rahmati, O., Golkarian, A., Biggs, T., Keesstra, S., Mohammadi, F., Daliakopoulos, I.N., 2019. Land subsidence hazard modeling: Machine learning to identify predictors and the role of human activities. J. Environ. Manage. 236, 466-480.

Riley, F.S., 1969. Analysis of borehole extensometer data from central California. International Association of Hydrologic Sciences Publication 89, 423-431.

Shang, R.-K., Shiu, Y.-S., Ma, K.-C., 2011. Using geographically weighted regression to explore the spatially varying relationship between land subsidence and groundwater level variations: a case study in the Choshuichi alluvial fan, Taiwan, Proceedings 2011 IEEE International Conference on Spatial Data Mining and Geographical Knowledge Services. IEEE, pp. 21-25.

Shearer, T., 1998. A numerical model to calculate land subsidence, applied at Hangu in China. Eng. Geol. 49, 85-93.

Shen, S.-L., Xu, Y.-S., 2011. Numerical evaluation of land subsidence induced by groundwater pumping in Shanghai. Canadian Geotechnical Journal 48, 1378-1392.

Sundell, J., Haaf, E., Norberg, T., Alen, C., Karlsson, M., Rosen, L., 2019. Risk mapping of groundwater-drawdown-induced land subsidence in heterogeneous soils on large areas. Risk Anal. 39, 105-124.

Teatini, P., Ferronato, M., Gambolati, G., Gonella, M., 2006. Groundwater pumping and land subsidence in the Emilia-Romagna coastland, Italy: Modeling the past occurrence and the future trend. Water Resour. Res. 42.

Tung, H., Hu, J.-C., 2012. Assessments of serious anthropogenic land subsidence in Yunlin County of central Taiwan from 1996 to 1999 by Persistent Scatterers InSAR. Tectonophysics 578, 126-135.

Xu, Y.-S., Shen, S.-L., Ren, D.-J., Wu, H.-N., 2016. Analysis of Factors in Land Subsidence in Shanghai: A View Based on a Strategic Environmental Assessment. Sustainability 8, 573.

Yan, T., Burbey, T.J., 2008. The value of subsidence data in ground-water model calibration. Ground Water 46, 438-450.

Yu, H.-L., Chu, H.-J., 2010. Understanding space–time patterns of groundwater system by empirical orthogonal functions: a case study in the Choshui River alluvial fan, Taiwan. J. Hydrol. 381, 239-247.

Zhang, Y., Gong, H., Gu, Z., Wang, R., Li, X., Zhao, W., 2014. Characterization of land subsidence induced by groundwater withdrawals in the plain of Beijing city, China. Hydrogeol. J. 22, 397-409.

Zhou, G., Esaki, T., Mori, J., 2003. GIS-based spatial and temporal prediction system development for regional land subsidence hazard mitigation. Environ. Geol. 44, 665-678.

Central Geological Survey: Project of groundwater monitoring network in Taiwan during first stage – research report of Choushui River alluvial fan, Water Resources Bureau press, Taipei County, 383 pp., 1999